RESEARCH ARTICLE

Southern Hemisphere mid- and high-latitudinal AOD, CO, NO$_2$, and HCHO: spatiotemporal patterns revealed by satellite observations

Dha Hyun Ahn[1], Taejin Choi[2], Jhoon Kim[1], Sang Seo Park[3], Yun Gon Lee[4], Seong-Joong Kim[2] and Ja-Ho Koo[1*]

Abstract

To assess air pollution emitted in Southern Hemisphere mid-latitudes and transported to Antarctica, we investigate the climatological mean and temporal trends in aerosol optical depth (AOD), carbon monoxide (CO), nitrogen dioxide (NO$_2$), and formaldehyde (HCHO) columns using satellite observations. Generally, all these measurements exhibit sharp peaks over and near the three nearby inhabited continents: South America, Africa, and Australia. This pattern indicates the large emission effect of anthropogenic activities and biomass burning processes. High AOD is also found over the Southern Atlantic Ocean, probably because of the sea salt production driven by strong winds. Since the pristine Antarctic atmosphere can be polluted by transport of air pollutants from the mid-latitudes, we analyze the 10-day back trajectories that arrive at Antarctic ground stations in consideration of the spatial distribution of mid-latitudinal AOD, CO, NO$_2$, and HCHO. We find that the influence of mid-latitudinal emission differs across Antarctic regions: western Antarctic regions show relatively more back trajectories from the mid-latitudes, while the eastern Antarctic regions do not show large intrusions of mid-latitudinal air masses. Finally, we estimate the long-term trends in AOD, CO, NO$_2$, and HCHO during the past decade (2005–2016). While CO shows a significant negative trend, the others show overall positive trends. Seasonal and regional differences in trends are also discussed.

Keywords: Climatology, Aerosol optical depth, Carbon monoxide, Nitrogen dioxide, Formaldehyde, Southern Hemisphere

Introduction

Antarctica is known as an isolated region due to its geographical distance from human activity, as well as the surrounding polar vortex hindering meridional exchange. However, some studies indicated the effective transport of air pollutants from the mid-latitudes to Antarctica in recent decades. For example, Pereira et al. (2004) and Neff and Bertler (2015) found that mineral aerosols can be transported from Patagonia to West Antarctica by a cyclonic system. Fiebig et al. (2009) and Hara et al. (2010) also suggested that observed aerosols at

Antarctic research stations can be attributed to the long-range transport from mid-latitudinal source regions in South America and Africa. Gorodetskaya et al. (2014) coined the phrase "atmospheric river" to describe this transport pathway between subtropical latitudes and Antarctica. In terms of atmospheric dynamics, the relationship between the mid-latitudinal and Antarctic atmospheric phenomena has been also examined (Gettelman et al. 2011).

Although these and several other studies have suggested a connection between the atmospheric environment in Antarctica and that in the mid-latitudes (Pereira et al. 2004; Fiebig et al. 2009; Hara et al. 2010), a detailed understanding is still poor, particularly for climatological variables. Since atmospheric compositional change in the polar region induces shifts in climatological patterns

* Correspondence: zach45@yonsei.ac.kr
[1]Department of Atmospheric Sciences, Yonsei University, Seoul, Republic of Korea
Full list of author information is available at the end of the article

(e.g., radiative forcing), the transport effects of air pollutants from the mid-latitudes should be further investigated. In fact, some simulations indicate that the polar region can experience a substantial change in atmospheric radiative forcing due to the impact of pollutant emissions from densely populated areas in the mid-latitudes (e.g., Streets et al. 2013). In addition, surface observations have revealed changes in polar physicochemical properties: carbon-based materials and even dust in the Antarctic region increased due to meridional transport (Li et al. 2008; Stohl and Sodemann 2010). Certainly, there are also some local anthropogenic emissions resulting in Antarctic pollution; for example, Antarctic power generation, trash burning, and vehicle, ship, and airplane transportation (Shirsat and Graf 2009; Graf et al. 2010). Nevertheless, a long-term background change over the broad Antarctic area is driven more by the influence of external air masses from the mid-latitudes. Therefore, determining the spatial distribution of air pollutants in the Southern Hemisphere and the typical transport routes to Antarctica is important (Bargagli 2008; McConnell et al. 2014).

Unfortunately, analysis based on ground-based observations in the Antarctic region is insufficient, to investigate the properties of pollutants in the Southern Hemisphere, due to spatial coverage limitations. Installation of new ground-based stations is also not an easy task because the Southern Hemisphere includes broader oceanic areas than the Northern Hemisphere. Application of model simulations could be an alternative way to overcome such limitations. However, ensuring reliable analysis is difficult because of the difficulty in performing validation, again due to the paucity of in situ measurements. In such a situation, satellite measurements seem to be quite useful for surmounting these limitations, but satellite data have their own uncertainty issues in the Southern Hemisphere, requiring careful application (McKenzie et al. 2001; Nazaryan et al. 2008). If we focus on the median pattern, which is free from outlier influence, then analysis of long-term satellite observations can assist in the investigation of climatological patterns and temporal trends.

For this purpose, we use long-term satellite measurements of aerosol optical depth (AOD), carbon monoxide (CO), nitrogen dioxide (NO_2), and formaldehyde (HCHO) to investigate climatological mean patterns, particularly spatiotemporal distributions and the long-term trends. Additionally, the back trajectory model results are used to investigate how mid-latitudinal particles and trace gases are transported to Antarctica. Through this analysis, we expect to diagnose whether changes in the mid-latitudinal atmospheric composition in the Southern Hemisphere tend to increase Antarctic air pollution.

Methods/Experimental
Data
Moderate resolution imaging spectrometer, aerosol optical depth, and fire count
The Aqua satellite, launched in 2002, crosses the equator at 13:30 local time (LT) on a sun-synchronous orbit. The Moderate Resolution Imaging Spectrometer (MODIS), a 36-channel radiometer aboard the Aqua satellite, observes irradiance with a spatial resolution of 250 m to 1 km in nadir viewing. Using this observation, AOD is retrieved based on dark target (DT) and deep blue (DB) algorithms, where DT is used for the measurement on dark surfaces such as the vegetative land and dark ocean, and DB is used for measurement on bright surfaces (Sayer et al. 2014). Surface condition is obtained from the MODIS climatology normalized difference vegetation index (NDVI) (Huete et al. 2010). In each algorithm, total AOD is estimated when the observed TOA reflectance matches TOA from the combination of the fine-mode-dominated aerosol model and the coarse-mode-dominated aerosol model at two wavelengths. Final AOD product is produced by averaging the results from DB and DT algorithms over land or from the DT algorithm over the ocean.

For this study's analysis, we use this final product, called the MODIS-Aqua Combined DT and DB AOD at 550 nm for the land and ocean (MYD08_M3_v6), which contains the high-quality assurance confidence flag (QAC) for each condition (Levy et al. 2013). The QAC value is determined by the number of valid pixels with screening cloud perturbations. Monthly mean values are generated based solely on data having reliable QAC values, meaning that our analysis is free from the cloud effect. Thus, this product can be used in this study without additional screening tasks. Most aerosols are produced near the surface and transported in the lower troposphere (Ocko and Ginoux 2017), hence AOD data can be used to investigate tropospheric characteristics in general.

Measurements of pollution in the troposphere: carbon monoxide
Measurements of Pollution in the Troposphere (MOPITT), a module aboard the Terra satellite, launched in 1999, has offered an observation dataset since 2000. The Terra satellite crosses the Equator at 10:30 and 22:30 LT on a sun-synchronous orbit, and MOPITT observes CO and methane (CH_4) with a field of view of 22 km × 22 km in nadir viewing (Deeter et al. 2003). MOPITT CO total column data are retrieved by three algorithms: TIR-only (exploiting the 4.7 μm thermal-infrared channel only), NIR-only (exploiting the 2.3 μm near-infrared channel only), and multispectral TIR-NIR (exploiting both thermal-infrared and near-infrared channels). The NIR-only CO product is

retrieved only over land. Meanwhile, the TIR-NIR multi-band product shows a relatively large random retrieval error and bias drift (Deeter et al. 2017), which are inappropriate for investigating the CO pattern over the Southern Hemisphere, where most of the ocean is located. Since the TIR-only product has uniform performance over the land and ocean (Deeter et al. 2017), the MOPITT TIR-only CO total column product (daytime and descending) (MOP03TM v007) is used in this study. MOPITT CO total columns show a sensitivity peak in the mid-troposphere, so using MOPITT CO data for tropospheric monitoring is reasonable (Kopacz et al. 2010; Yurganov et al. 2011). We do not consider monthly products for August and September 2009 in the analysis due to a calibration issue from 28 July 2009 to 28 September 2009.

Ozone monitoring instrument, nitrogen dioxide, and formaldehyde

The Ozone Monitoring Instrument (OMI) is an ultraviolet (UV)–visible (Vis) spectrometer aboard the NASA-EOS Aura satellite, launched in 2004 on a sun-synchronous polar orbit. The Aura satellite crosses the Equator at 13:38 LT on a sun-synchronous orbit. OMI has a spectral resolution of 0.45–1.0 nm at three channels in the range of 270 nm to 500 nm (270–314 nm, 306–380 nm, and 350–500 nm) and obtains global coverage every day with a cross-track swath of 2600 km. The spatial resolution is 13 km × 24 km in nadir viewing, decreasing to 28 km × 150 km near the edge of the swath; this feature is an improvement compared to the Total Ozone Mapping Spectrometer (TOMS) and Global Ozone Monitoring Experiment (GOME). OMI continues to monitor ozone (O_3) and trace gases, such as nitrogen dioxide (NO_2), sulfur dioxide (SO_2), formaldehyde (HCHO), bromine monoxide (BrO), and chlorine dioxide (OClO).

The OMI NO_2 vertical column density (VCD) is calculated by applying the air mass factor (AMF) to the slant column density (SCD) obtained using the differential optical absorption spectroscopy (DOAS) method. The tropospheric column is retrieved when the VCD exceeds the value of the estimated stratospheric field. Then, the VCD is recalculated using AMF information acquired from the assumed tropospheric NO_2 profile (Bucsela et al. 2006). Finally offered after quality screening is the level 3 product, which is the monthly NO_2 tropospheric column averaged from the OMI level 3 daily global gridded (0.25° × 0.25°) nitrogen dioxide product (OMNO2d v003). Only daily products with a cloud fraction < 0.3 are used to calculate the monthly product.

Similarly, for the retrieval of tropospheric OMI HCHO VCD, OMI HCHO SCD is first obtained using the DOAS method. Then, the tropospheric HCHO SCD is generated by subtracting the stratospheric HCHO SCD from the total HCHO SCD. The stratospheric HCHO SCD is generally obtained by choosing a reference sector, which is the pixel showing the background concentration, free from tropospheric pollution. Here, this reference sector is chosen in the center of the Pacific Ocean (140–160° W). Since there can be an overestimation or underestimation of stratospheric HCHO SCD in this process, complementary post-processing is performed using the background tropospheric HCHO simulated from 3D-CTM IMAGES (De Smedt et al. 2012; De Smedt et al. 2015; Stavrakou et al. 2009). Finally, this modified tropospheric HCHO SCD is converted to tropospheric HCHO VCD by applying tropospheric AMF. The Belgian Institute for Space Aeronomy (BIRA-IASB) offers the OMI tropospheric HCHO VCDs that have passed through a quality check. The L3 monthly product is calculated only from daily products showing a cloud fraction < 0.4 and a solar zenith angle < 70°. However, OMI HCHO data still show large uncertainties. Sometimes data are unavailable, particularly during the austral winter (June-July-August).

Hybrid single-particle Lagrangian integrated trajectory back trajectory model

A back trajectory analysis is used to investigate the transport of aerosols and trace gases from the mid-latitudes to Antarctica. The National Oceanic and Atmospheric Administration (NOAA) Air Resources Laboratory developed the Hybrid Single-Particle Lagrangian Integrated Trajectory (HYSPLIT) model to simulate the movement of air parcels (Stein et al. 2015). For inspecting the pathways of potential air mass transport to Antarctica, we calculate 10-day back trajectories using the HYSPLIT version 4 model, based on meteorology fields from the National Centers for Environmental Prediction and National Center for Atmospheric Research reanalysis data. Back trajectories are calculated at six stations located along the Antarctic coast: King Sejong (62.22° S, 58.79° W), Belgrano II (77.87° S, 34.63° W, hereafter Belgrano), Neumayer (70.68° S, 8.27° W), Syowa (69.00° S, 39.58° E), Davis (68.58° S, 77.97° E), and Jangbogo (74.62° S, 164.23° E) stations. Back trajectories are calculated twice a day (00 and 12 UTC), from 2005 to 2016, and each back trajectory has a 1-km arrival height above ground level.

Climatological mean

Based on the analysis of satellite data in the mid-latitudes with interpretation of back trajectory patterns, we can diagnose the impact of meridional transport to the Antarctic atmosphere. The climatological mean is one of the representative patterns that we can investigate. Unfortunately, satellite data often show large uncertainties over Southern Hemisphere mid-latitudes

(McKenzie et al. 2001; Nazaryan et al. 2008) because of the low amplitude and large sampling error induced by frequent cloud occurrences (Zhang et al. 2005). Nevertheless, a representative climatological mean can be calculated by eliminating outliers. A median is an appropriate parameter to assess the typical climate without the influence of abnormal outliers. Therefore, we first find the median in each designated region, with regions defined with sufficient latitudinal breadth to include sufficient data. For this objective, the mid-latitude region in the Southern Hemisphere (30–60° S) is divided into 48 areas to obtain pixels with a size of longitudinal 45° × latitudinal 5°. Then, the median value is determined for each month and is considered the representative value for that area for that month. The climatological monthly mean is finally obtained by averaging all monthly values from 2005 to 2016 for each area.

Trend estimation
To show long-term variation in AOD, CO, NO_2, and HCHO, we use the representative monthly values for each area from 2005 to 2016. Generally, variations in atmospheric aerosols and trace gases contain strong seasonal variations. Thus, deseasonalization of the data should be conducted first. We use a time-series of anomalies for the trend analysis, obtained by subtracting monthly climatological values from the monthly median time-series. We perform the trend analysis based on the detailed methodology in Weatherhead et al. (1998), De Meij et al. (2012), and Hsu et al. (2012). The entire process of our trend analysis is summarized below.

First, we use the given data to construct a simple linear trend model,

$$Y_t = \mu + \omega X_t + N_t, t = 1, \cdots, T \qquad (1)$$

where Y_t is the time-series of target variables, μ is an offset term, ω is the linear trend (year^{-1}), and X_t is the time. In this study, t represents each month, and X_t is defined as $t/12$. The last term, N_t, is the noise term and represents the residual of the time-series and the fitting line. Generally, meteorological factors have autoregressive properties; therefore, we assumed an autoregressive model with a lag of 1 month. The noise term can be expressed as follow:

$$N_t = \phi N_{t-1} + \varepsilon_t \qquad (2)$$

where ϕ is the autoregressive coefficient and ε_t is the random noise.

Evaluating whether the estimated trend is significant is another essential task for the trend analysis. To examine the significance of the linear trend ω, the uncertainty (σ_w) of the trend is calculated as follows:

$$\sigma_w \approx \frac{\sigma_N}{n^{3/2}} \sqrt{\frac{1+\varnothing}{1-\varnothing}} \qquad (3)$$

where σ_N is the standard deviation of the noise and n is the total number of years of the time-series. The significance of the trend can be tested by the ratio of the linear trend slope to the uncertainty ($|\omega/\sigma_\omega|$). The trend is significant at the 95% confidence level if the ratio exceeds 1.96 or at the 90% level if the ratio exceeds 1.65. Each criterion is based on the z-score of each level point of the normal distribution (Hsu et al. 2012).

Equation (1) is also used to calculate the linear trend of the seasonal time-series. The seasonal time-series consists of the consecutive series of monthly medians in each season (Hsu et al. 2012). Since the seasonal time-series has an irregular temporal resolution, a Student's t test is used to compute the trend significance instead of Eq. (3). The p value is computed from the F ratio, which is defined as the ratio of regression mean squared error to the residual mean squared error. In general, the trend is considered significant at the 95% confidence level when the p value is less than 0.05.
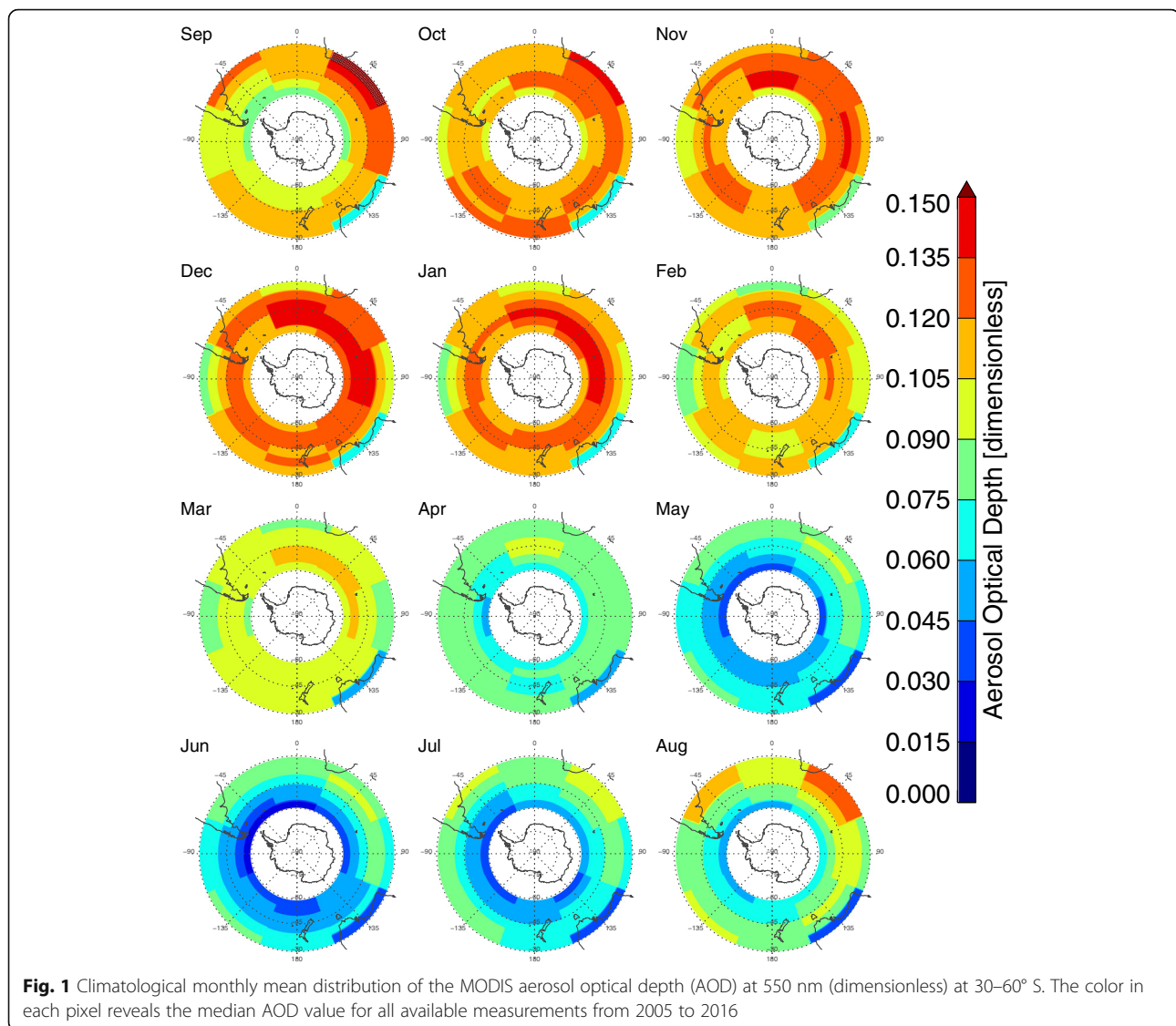
Results and discussion
Climatological mean patterns
Aerosol optical depth
The distribution of the climatological monthly mean of AOD is shown in Fig. 1. AOD is generally high in the austral spring (September-October-November, SON) and summer (December-January-February, DJF) but low in the austral autumn (March-April-May, MAM) and winter (June-July-August, JJA). This pattern is similar to that found in previous studies (Torres et al. 2002; Ocko and Ginoux 2017). In Africa, the AOD maximum occurs in September, consistent with the season of peak biomass burning in Africa (Das et al. 2017). The monthly distribution in South America has the same pattern as in Africa, also indicating the likely contribution of biomass burning to the level of AOD. Annual AODs in Australia are lower compared to the other continents because of the relatively low contribution of biomass burning. Instead, AOD monthly variation in Southern Australia (Fig. 1) can be affected more by dust. Prospero et al. (2002) mentioned that dust storms in Australia begin in September and October, reach a maximum in December to February, and end in May. This can explain the pattern of high Australian AOD from September to November.

For each season, the high or low patterns of AOD in the high-latitude regions seem to coincide with the variation in the mid-latitude regions, particularly near the continents (Mao et al. 2014; Mehta et al. 2016). Thus, the idea that aerosols in the mid-latitudes are diffused and transported to high latitudes can be inferred. We

Fig. 1 Climatological monthly mean distribution of the MODIS aerosol optical depth (AOD) at 550 nm (dimensionless) at 30–60° S. The color in each pixel reveals the median AOD value for all available measurements from 2005 to 2016
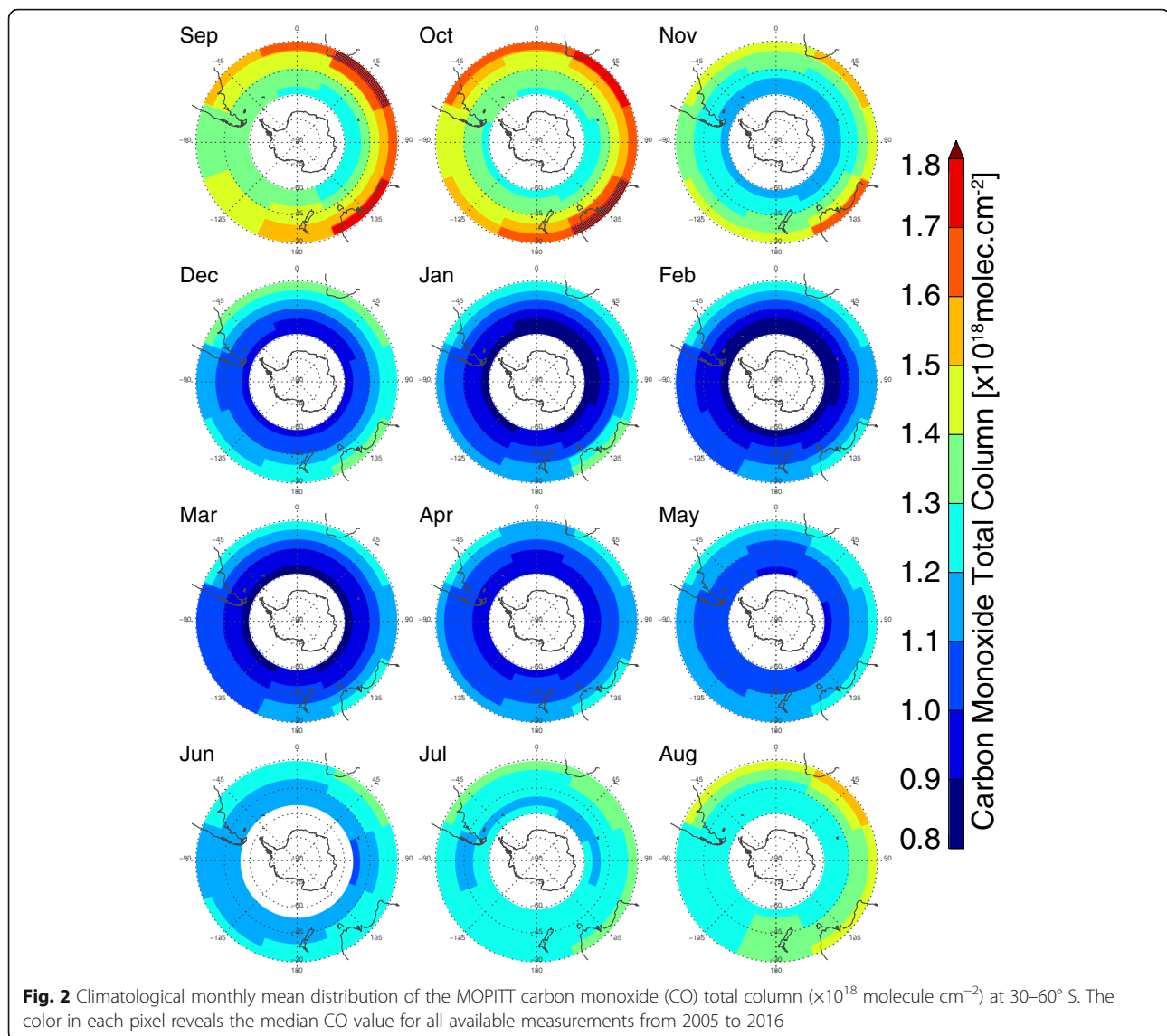
also find AOD enhancement over the ocean. AOD levels in some oceanic areas are comparable to those in continental regions, particularly over the Southern Atlantic Ocean (22.5° W to 22.5° E, 45° S to 55° S) (Fig. 1). High AOD in this region can be explained by active sea salt production driven by strong winds (Additional file 1: Figure S1) (Kishcha et al. 2009; Wilson et al. 2010). The high AOD in this region might also result in part from cloud influence (Kishcha et al. 2009) and from the relatively short distance from the source compared to other high-latitude regions (Mao et al. 2014).

Carbon monoxide

Generally, fossil fuel emission is a major source of global CO (Holloway et al. 2000). In the Southern Hemisphere, CO is dominantly emitted from biomass burning events. Thus, the CO concentration largely relates to the

frequency of fire events. The long lifetime of CO, about 1 month in the troposphere (Wang et al. 1997), also enables us to monitor the spatial characteristics of air mass transport. From the climatological monthly mean distribution of the CO column (Fig. 2), we can detect major source regions of CO in Africa, Australia, and South America. Researchers know that CO levels become enhanced over biomass burning sites in Africa and South America (Mok et al. 2017). Therefore, the high continental CO concentration in SON and JJA relates to active biomass burning in the dry season (Edwards et al. 2006; Torres et al. 2010). The region of Australia includes sources of both the burning of biomass (Das et al. 2017) and fossil fuel combustion in urbanized areas (Lamarque et al. 2010; Té et al. 2016). In fact, anthropogenic emissions have recently been found to make an important contribution to the CO concentration (Hooghiemstra et

Fig. 2 Climatological monthly mean distribution of the MOPITT carbon monoxide (CO) total column ($\times 10^{18}$ molecule cm^{-2}) at 30–60° S. The color in each pixel reveals the median CO value for all available measurements from 2005 to 2016

al. 2012). Since CO is mostly emitted from continental sources, CO levels over the Antarctic gradually decrease with increasing distance from the source regions. However, some high CO concentrations can be found over the ocean; we attribute these instances to the transport of CO from emission sources.

Nitrogen dioxide

NO_2 is a trace gas usually emitted from anthropogenic sources such as vehicles and power plants (Beirle et al. 2003; McDonald et al. 2012). Spatiotemporal patterns of NO_2 are generally helpful for monitoring the magnitude of air pollution in urban areas. The climatological monthly mean distribution of OMI tropospheric NO_2 is shown in Fig. 3. Similar to that of CO, the distribution of tropospheric NO_2 shows enhancement in continental mid-latitudes in Africa, South America, and Australia.

This is because NO_2 is emitted not only from urban areas but also from the burning of biomass (Beirle et al. 2003). In general, NO_2 maxima occur in winter over Australia and in winter and early spring over Africa and South America (van der et al. 2008). In line with those findings, we find a NO_2 peak in the JJA period over the Southern Hemisphere. Among the three continental regions, NO_2 concentrations were higher in Australia (generally $> 4.0 \times 10^{14}$ molecules/cm^2) than in Southern Africa (generally $> 2.5–3.0 \times 10^{14}$ molecules/cm^2) or in South America (generally $3.0–3.5 \times 10^{14}$ molecules/cm^2), ostensibly due to anthropogenic sources. Although NO_2 has a short average lifetime, on the order of 1 day (Beirle et al. 2003), the distribution of high NO_2 around the source regions indicates that NO_2 can be transported away from source regions. The transport of NO_2 can occur in the form of reservoirs, such as peroxyacetyl
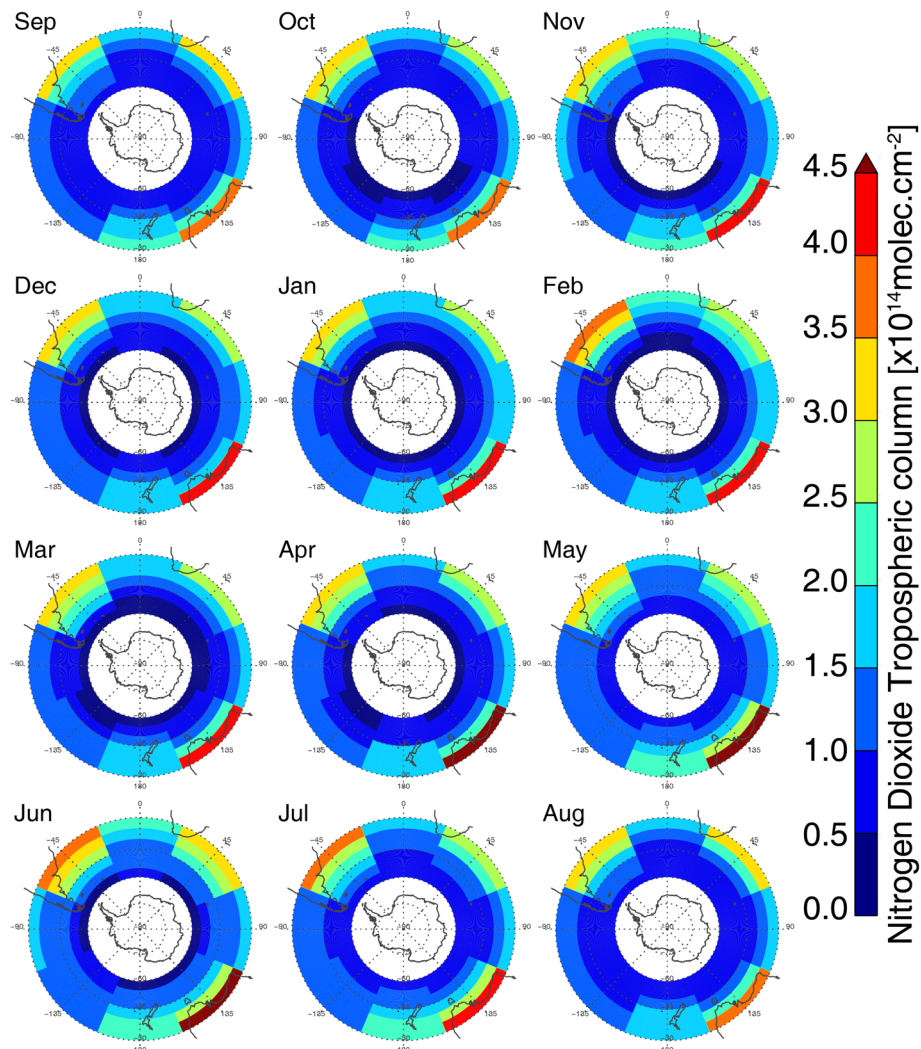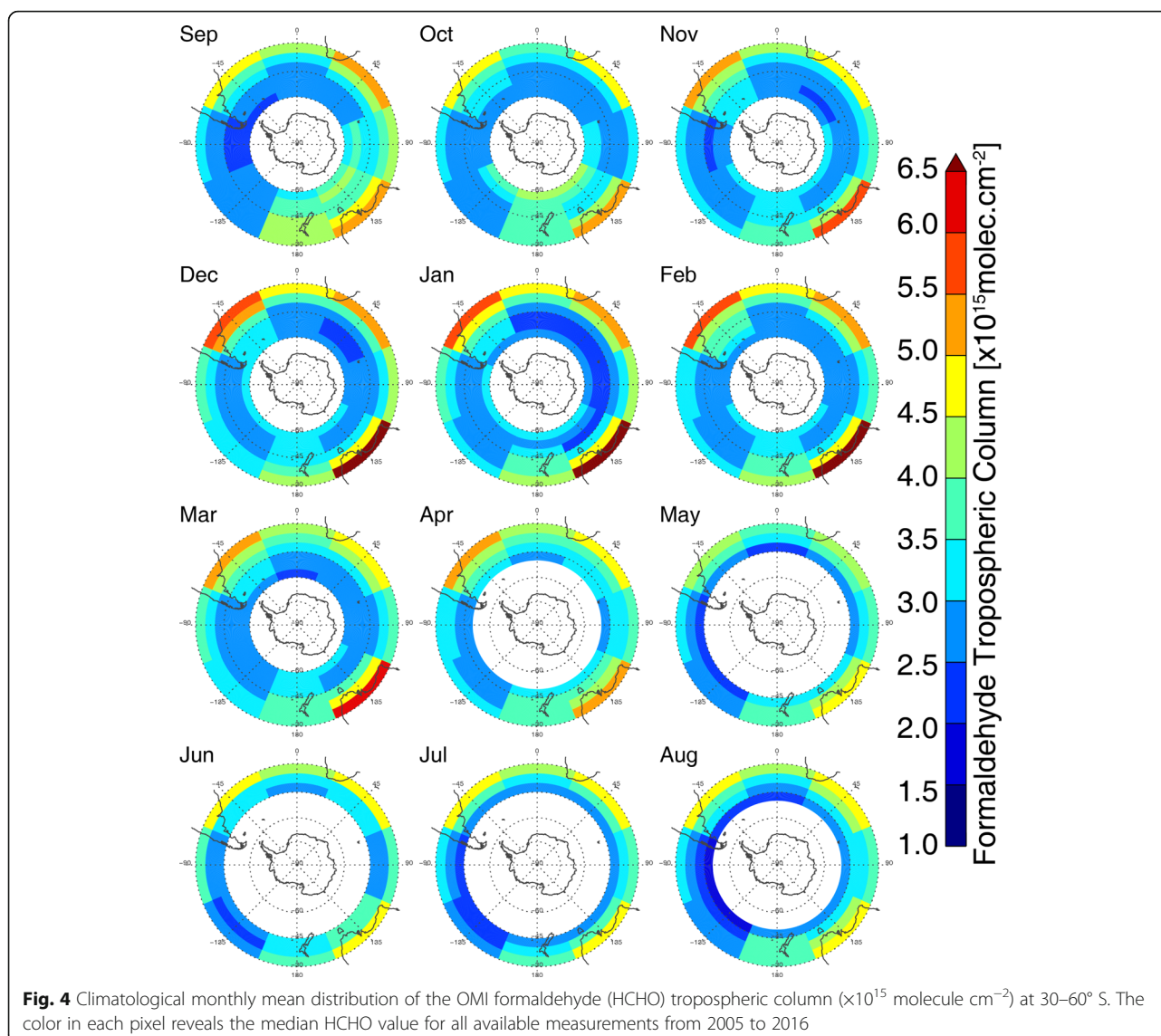
Fig. 3 Climatological monthly mean distribution of the OMI nitrogen dioxide (NO_2) tropospheric column ($\times 10^{14}$ molecule cm^{-2}) at 30–60° S. The color in each pixel reveals the median NO_2 value for all available measurements from 2005 to 2016

nitrates (PANs) (Liu et al. 2003; Zhu et al. 2017). The higher the latitude within the study area, the lower the concentration of NO_2, again illustrating the absence of NO_2 sources (e.g., urban and industry) near the polar region.

Formaldehyde

The monthly distribution of the OMI tropospheric HCHO column is shown in Fig. 4. HCHO is usually produced from the oxidation of CH_4 and other hydrocarbons (Wagner et al. 2002; Palmer et al. 2006). Thus, high HCHO levels can be found in regions where forests, biomass burning sources, industrial complexes, and vehicle traffic are located. As reported above for AOD, CO, and NO_2, the highest HCHO levels are found over the continents of Africa, South America, and Australia.

Seasonally, HCHO starts to increase in SON, peaks in DJF, and decreases after March, reaching a minimum in JJA. HCHO produced by the photochemical breakdown of CH_4 and hydrocarbons (Leuchner et al. 2016) relates to the summer peak, when the solar irradiance is high. Additionally, this annual pattern appears to generally follow seasonal cycles of biogenic emission and biomass burning (Dufour et al. 2009). The spatial HCHO distribution (Fig. 4) appears to be analogous to the NO_2 distribution (Fig. 3), similar to the known relationship between HCHO and NO_x (Jones et al. 2009). Therefore, high HCHO concentration in Australia can be also explained by the high NO_2 emission from the urban region, as discussed above. Since isoprene can also be a precursor of HCHO (Guenther et al. 2006), future work should investigate the relationship of HCHO to isoprene

Fig. 4 Climatological monthly mean distribution of the OMI formaldehyde (HCHO) tropospheric column (×10^{15} molecule cm^{-2}) at 30–60° S. The color in each pixel reveals the median HCHO value for all available measurements from 2005 to 2016

in the whole Southern Hemisphere, although such an investigation cannot feasibly be easily performed at present using satellite measurements alone.
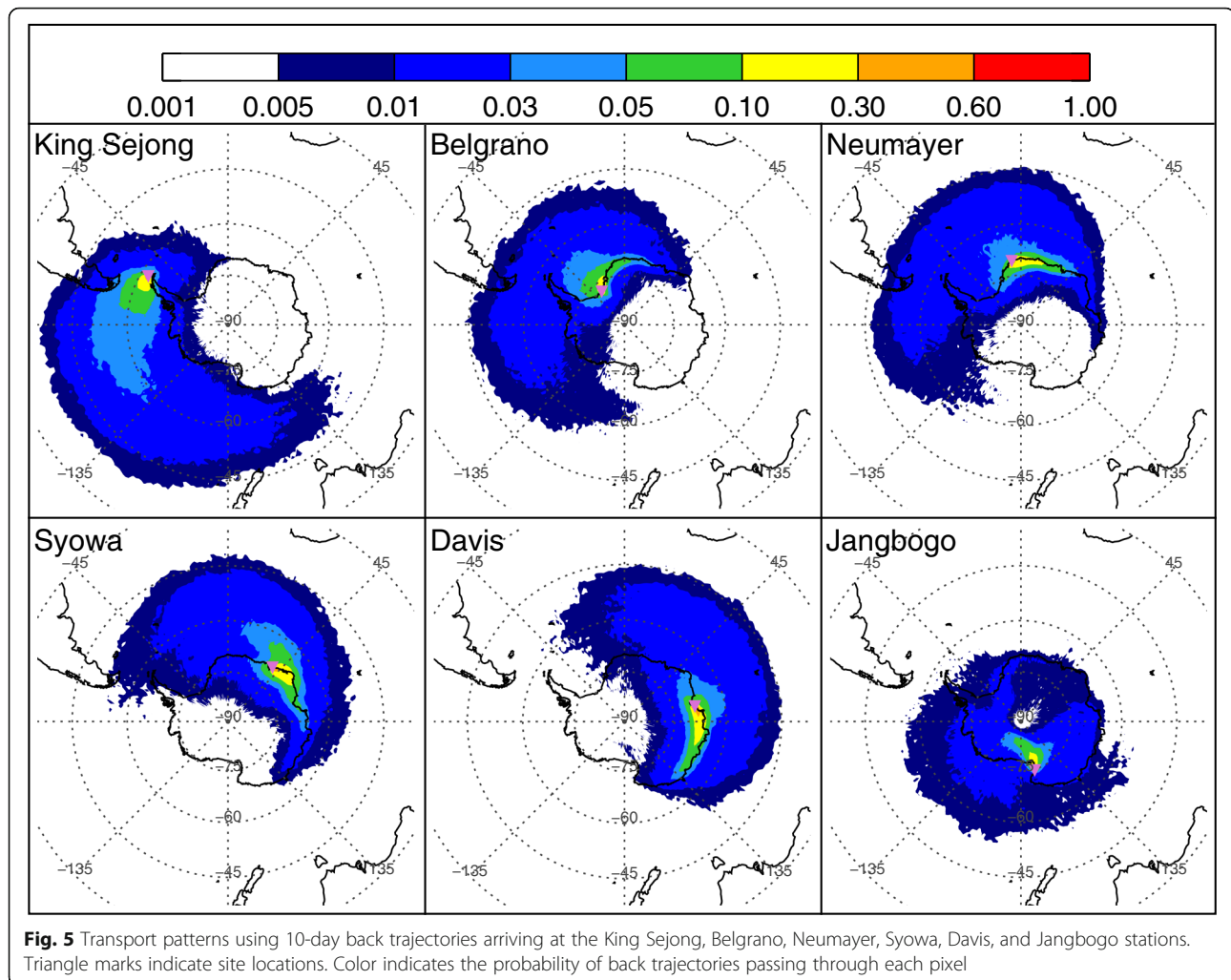
All the above interpretations need to be carefully considered because of the uncertainty of HCHO retrieval attributed to relatively weak signals and a strong interference (Li et al. 2015). Thus, the improvement of the HCHO retrieval algorithm is another future undertaking required for a better understanding of climatological HCHO patterns.

Transport patterns from the mid-latitudes to Antarctica
In this study, one of the most important reasons for examining the atmospheric composition in the Southern Hemisphere is to estimate the influence of mid-latitudinal pollution on the Antarctic environment. Here, we investigated back trajectory results along with the climatological

characteristics of the atmospheric constituents (Figs. 1, 2, 3, and 4), in order to evaluate the transport impact of mid-latitudinal pollutants. Specifically, we analyzed the back trajectory patterns at some representative ground stations with a long-term operation in the Antarctic region. Among all possible ground stations located in the coastal region around Antarctica, we selected six relatively evenly spaced stations to cover the Antarctic region evenly: the King Sejong, Belgrano, Neumayer, Syowa, Davis, and Jangbogo stations (Additional file 1: Figure S2).

The spatial frequencies of all 10-day back trajectories for each station are depicted in Fig. 5. The overall transport pattern reveals that all stations except the Jangbogo station can be affected by the transport of air masses from outside Antarctica. Basically, this transport pattern appears along the border of the polar vortex that encircles Antarctica; however, some pathways indicate the

Fig. 5 Transport patterns using 10-day back trajectories arriving at the King Sejong, Belgrano, Neumayer, Syowa, Davis, and Jangbogo stations. Triangle marks indicate site locations. Color indicates the probability of back trajectories passing through each pixel

inflow of mid-latitudinal air masses. Compared to the height of back trajectories from the inner Antarctic continent (Additional file 1: Figure S3), the height of back trajectories from the mid-latitudes is lower (Additional file 1: Figure S4), mostly trapped below 2 km for 10 days. This feature shows the real contribution to the Antarctic area of the near-surface air conditions in the mid-latitudes. The King Sejong station, located in the western Antarctic peninsula, clearly shows the direct influence of air masses originating from the southern part of South America. This station is also affected by air parcels from the south of Australia on a timescale of 10 days. These findings are supported by several previous studies showing that the Antarctic peninsula is relatively more polluted than the rest of Antarctica (Pereira et al. 2004; Bargagli 2008).

The King Sejong station is not the only station showing such influence; the Belgrano, Neumayer, and Syowa stations also show some back trajectories from South America on a timescale of 10 days. Thus, these sites also

appear affected by the transport of air pollutants from South America. In contrast, most back trajectories arriving at the Jangbogo station come from the inner region of Antarctica, particularly the eastern Antarctic plateau (Fig. 5). The strong katabatic flow from the eastern Antarctic plateau appears to cause this back trajectory pattern (Parish 1992). Thus, the Jangbogo station, located downwind of the eastern Antarctic plateau, appears to be far from the influence of mid-latitudinal pollutants. The Davis station, located in East Antarctica, also does not show 10-day back trajectories originating from the continental mid-latitudes. Since significant transport of air pollutants is usually expected in 10 days (e.g., Hara et al. 2010), the Davis station also appears to be less affected by mid-latitudinal pollutants than other stations (The King Sejong, Belgrano, Neumayer, and Syowa stations).

In brief, the western part of Antarctica shows more intrusion of mid-latitudinal pollutants than the eastern part of Antarctica, as found in a previous study (Tomasi

et al. [2015]). Considering the climatological distributions of AOD, CO, NO_2, and HCHO simultaneously (Figs. [1], [2], [3], and [4]), air pollutants emitted in South America seem to have a larger effect on Antarctica than do those emitted elsewhere. In contrast, air pollutants from Southern Africa might not contribute to the Antarctic atmosphere greatly because even the eastern Antarctic coast closest to Africa is relatively isolated due to the stronger zonal advection, as illustrated by back trajectories. In fact, the climatological mean wind speed at 850 hPa (Additional file [1]: Figure S1) well illustrates that the zonal wind speed is higher around East Antarctica (> 16 m/s at maximum) than west Antarctica (< 13 m/s at maximum). Considering that AOD is greatly enhanced over the southern Atlantic region (Fig. [1]), however, emissions in Southern Africa can also have some effect on the Antarctic atmosphere when the zonal wind becomes weak; this possibility is consistent with the discussion in Hara et al. ([2010]).

Trend analysis

Based on the methodology of the trend estimation suggested above, we calculate the 12-year deseasonalized trend of satellite-observed AOD, CO, NO_2, and HCHO. Time-series trends for whole mid-latitudes in the Southern Hemisphere (30–60° S) show moderate increases in AOD, NO_2, and HCHO but a decrease in CO (Fig. [6]). To examine regional trends, we analyze all time-series for each pixel with a size of 45° longitude × 5° latitude (e.g., Additonal file [1]: Figure S5). We summarize trend

values with uncertainties (1-sigma) in Figs. [7], [8], [9], and [10] and in Additional files [1]: Tables S1–S4. Findings are described in detail below.

Aerosol optical depth

Figure [7] shows that overall AOD in the mid-latitudes of the Southern Hemisphere tends to increase regardless of the season, a finding consistent with previous studies (De Meij et al. [2012]; Hsu et al. [2012]). Figure [7] illustrates the high AOD peak in 2015–2016, which highlights the positive trend in AOD. However, when individual pixels are examined, AOD in 2015–2016 does not appear strikingly high compared to other periods (e.g., Additional file [1]: Figure S5). This finding implies that the mean mid-latitudinal AOD trend over the whole Southern Hemisphere is not necessarily representative of regional AOD trends. In the spatial trend analysis, we find a strong positive trend in SON and DJF in the Southern Atlantic Ocean, where strong winds are present and thus where high AOD is found (Fig. [1]). This positive trend might be associated with an enhanced frequency or intensity of sea salt production (Kishcha et al. [2009]). In fact, we find a secular increase in the tendency for 850 hPa wind speed over the Southern Atlantic Ocean (Additional file [1]: Figure S6); this increase would be expected to enhance AOD by way of wind-driven sea salt generation from the ocean surface. In JJA, a positive trend appears overall around Antarctica, as shown by Mehta et al. ([2016]). These positive trends are found in both mid-latitudes and high latitudes (Additional file [1]: Table S1), implying that future
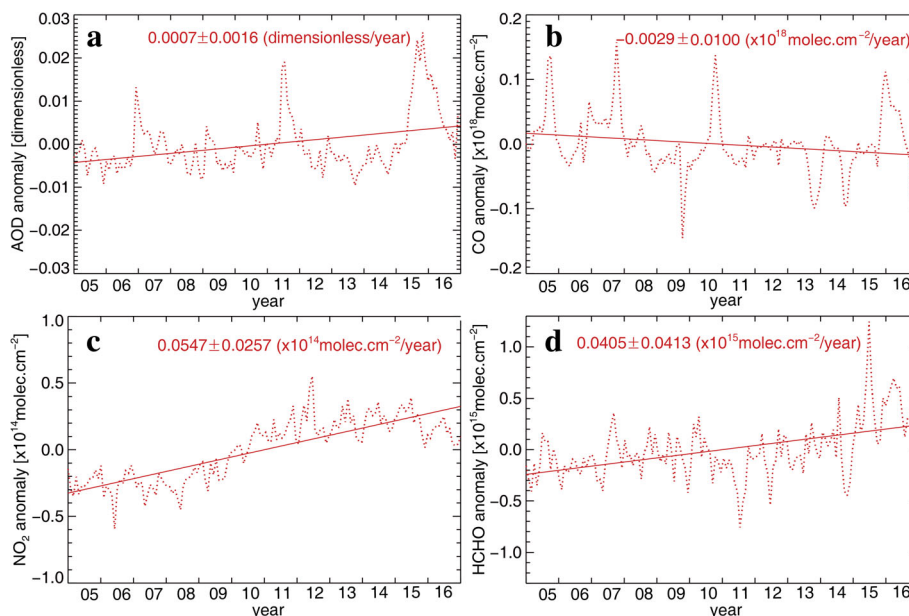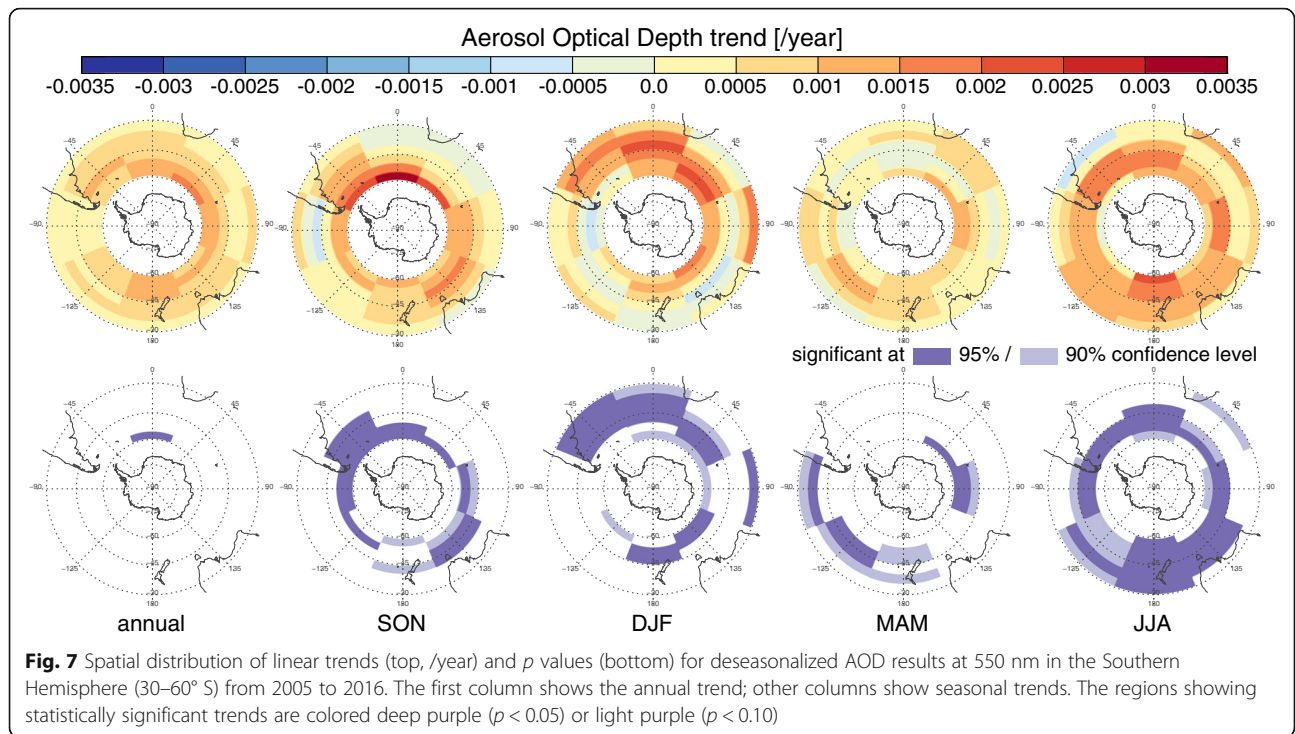

Fig. 6 Time-series (dotted line) and the linear trend (solid line) of monthly mean deseasonalized anomalies of **a** AOD at 550 nm, **b** CO total column density, **c** NO_2 tropospheric column density, and **d** HCHO tropospheric column density. All measures are for the Southern Hemisphere (30–60° S) from 2005 to 2016
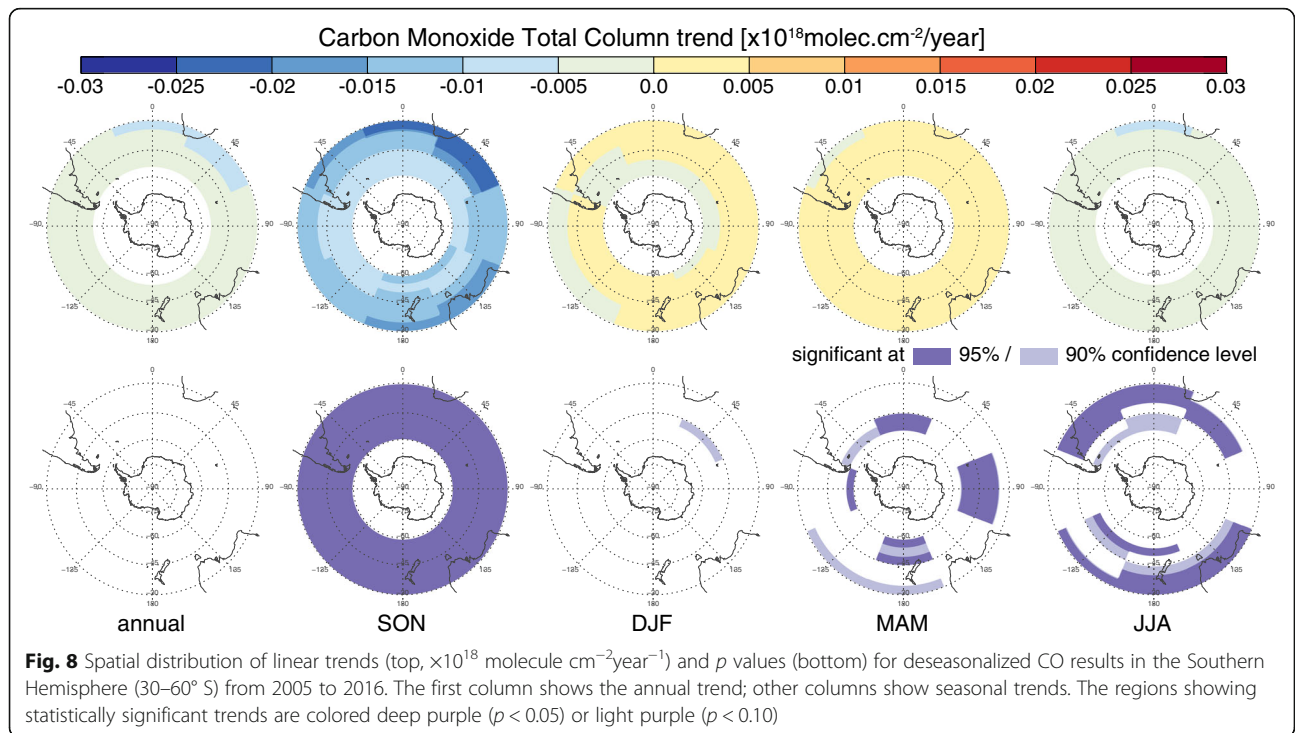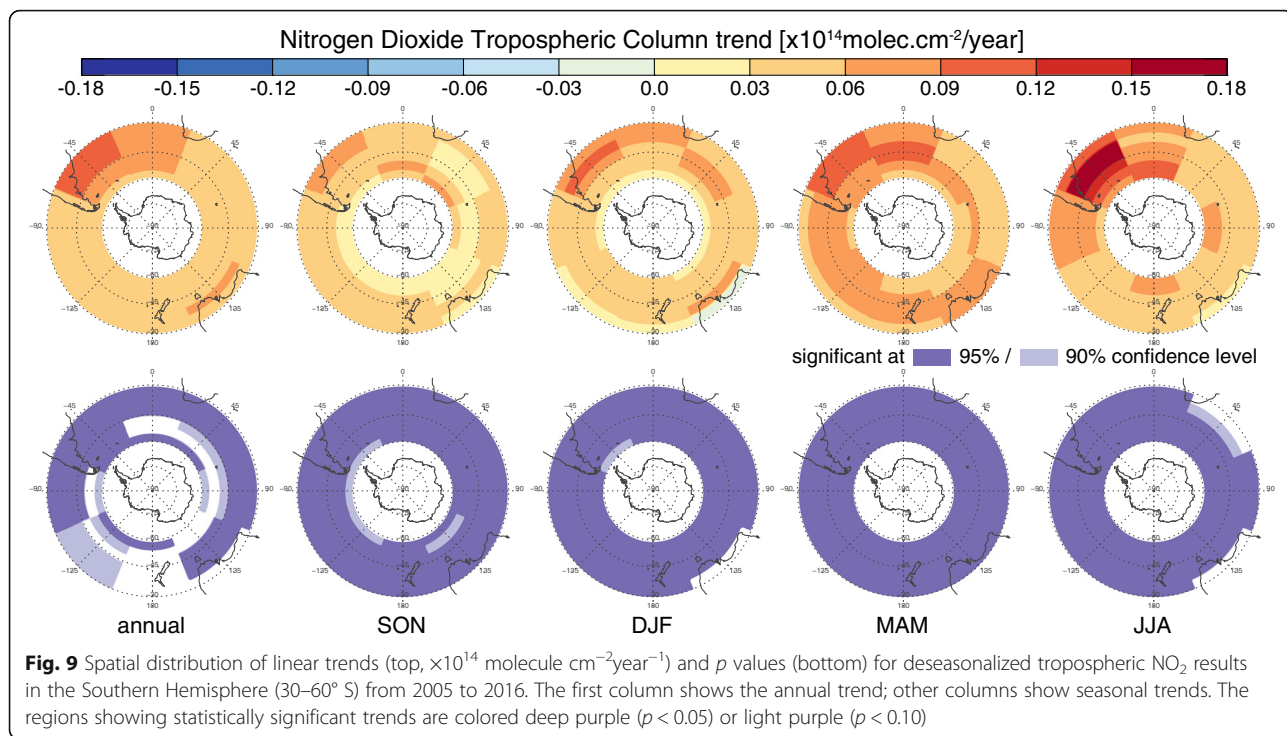
Fig. 7 Spatial distribution of linear trends (top, /year) and *p* values (bottom) for deseasonalized AOD results at 550 nm in the Southern Hemisphere (30–60° S) from 2005 to 2016. The first column shows the annual trend; other columns show seasonal trends. The regions showing statistically significant trends are colored deep purple (*p* < 0.05) or light purple (*p* < 0.10)

AOD levels in Antarctica may increase by means of the meridional transport effect.

Carbon monoxide

Secular and seasonal linear trends for CO are provided in Fig. 8 and Additional file 1: Table S2. The secular data

show a weakly negative trend throughout the Southern Hemisphere, although without apparent statistical significance. However, in the seasonal analysis, some linear trends of statistical significance are found, the most prominent being the strong decrease in SON. This large CO decrease in SON dominates the annual CO
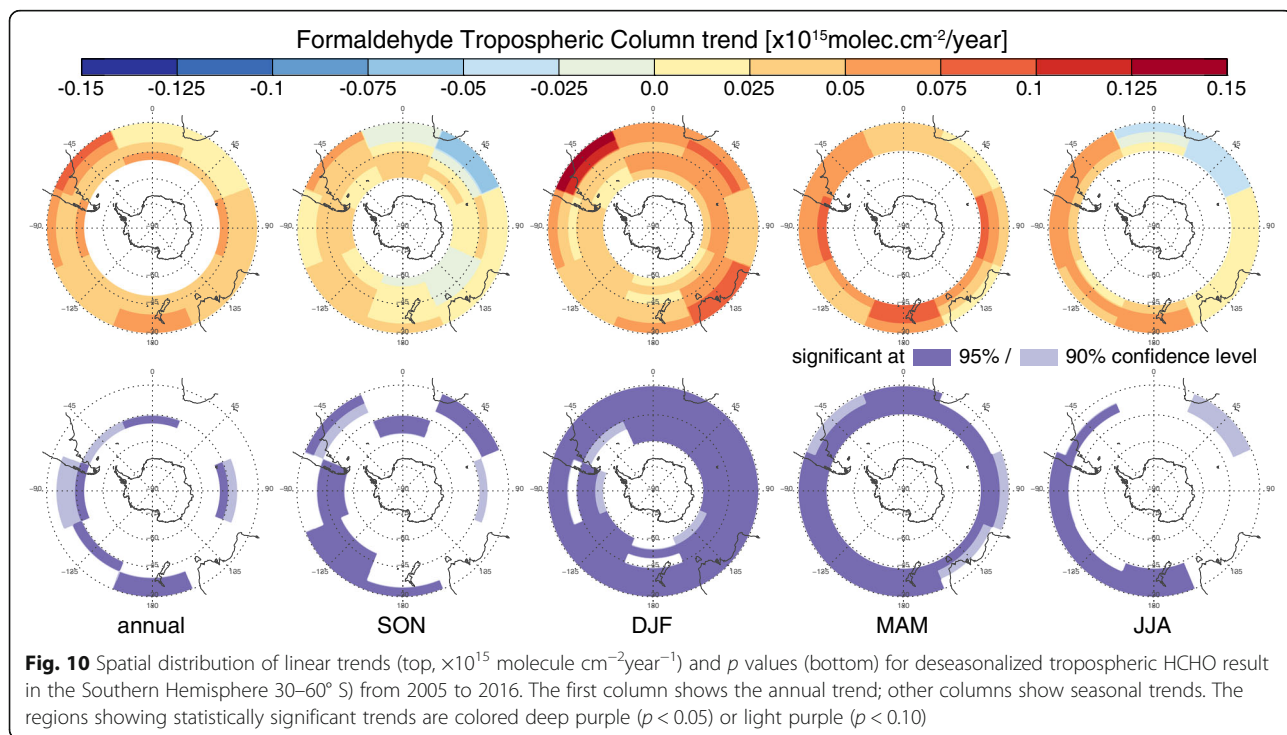

Fig. 8 Spatial distribution of linear trends (top, ×10^18 molecule cm^−2 year^−1) and *p* values (bottom) for deseasonalized CO results in the Southern Hemisphere (30–60° S) from 2005 to 2016. The first column shows the annual trend; other columns show seasonal trends. The regions showing statistically significant trends are colored deep purple (*p* < 0.05) or light purple (*p* < 0.10)

Fig. 9 Spatial distribution of linear trends (top, $\times 10^{14}$ molecule cm^{-2}year^{-1}) and p values (bottom) for deseasonalized tropospheric NO_2 results in the Southern Hemisphere (30–60° S) from 2005 to 2016. The first column shows the annual trend; other columns show seasonal trends. The regions showing statistically significant trends are colored deep purple ($p < 0.05$) or light purple ($p < 0.10$)

decrease, more than making up for the weak positive trend in DJF and MAM. These negative trends in CO concentration in the Southern Hemisphere have been explained by decreases in anthropogenic emissions and biomass burning events (Zeng et al. 2012; Worden et al. 2013). CO decrease is particularly remarkable on the

continents, where biomass burning sources occur. Southern Africa, for example, shows the largest negative trend.

In order to diagnose biomass burning activity, we next examine total fire counts over South America, Africa, and Australia (Additional file 2). Despite the large

Fig. 10 Spatial distribution of linear trends (top, $\times 10^{15}$ molecule cm^{-2}year^{-1}) and p values (bottom) for deseasonalized tropospheric HCHO result in the Southern Hemisphere 30–60° S from 2005 to 2016. The first column shows the annual trend; other columns show seasonal trends. The regions showing statistically significant trends are colored deep purple ($p < 0.05$) or light purple ($p < 0.10$)

annual variation, the fire count has recently shown a decreasing tendency (Additional file 1: Figure S7), implying a possible relationship with the observed CO decrease. Also, Additional file 1: Figure S7 indicates that the fire count (i.e., biomass burning emissions) has been decreasing since 2009 and 2010. Given the significant influence of transported biomass burning on CO temporal variation in the Southern Hemisphere (Zeng et al. 2012), the negative trend in fire counts since 2009 and 2010 may be intensifying a persistent negative CO trend. In other words, the negative trend in fire counts strongly indicates that biomass burning plays an important role in declining CO trends for the period studied here (2005–2016). Though suggestive, this attribution needs to be further explored using mechanistic models. Considering the relationship between AOD and biomass burning discussed above, the question of how a reduction in fire counts can explain both AOD increases and CO reductions at the same time is not clear. Future work should consider whether other emission sources (e.g., anthropogenic emission) might show different temporal patterns.

Nitrogen dioxide and formaldehyde

Tropospheric NO_2 trends generally increase with a high statistical significance (Fig. 9 and Additional file 1: Table S3). All annual and seasonal trends are consistently positive, but the positive trend in the southern part of South America is even clearer than those of other regions. This result relates to a previous finding regarding tropospheric NO_2 growth patterns in South America (Schneider et al. 2015). This tropospheric NO_2 growth pattern is caused by an increase in air pollutants, due to urbanization (Lamsal et al. 2013). The strongest positive trends in the winter might be related to increased anthropogenic energy consumption, as well as to reduced NO_2 photolysis rate in the winter. Considering the large intrusion of air masses from South America to the western part of Antarctica, particularly at the King Sejong station (Fig. 5), we presume that the snow NO_x concentration over the western Antarctic region might show a gradual increase in the future, due to the transport of nitrogen compounds (e.g., HNO_3). So far, anthropogenic pollutants in the mid-latitudes do not seem to influence the Antarctic atmospheric compositional variation (Weller et al. 2011), but such effects may appear if global anthropogenic emissions continue to increase (Weller et al. 2013).

Though not as dramatic and pervasive as tropospheric NO_2, tropospheric HCHO generally shows a positive trend in the mid-latitudes of the Southern Hemisphere (Fig. 10 and Additional file 1: Table S4). The largest HCHO increase occurs in South America, particularly during DJF, which coincides with strong photochemical production in the summer. This positive trend in South America might be the result of an increase in anthropogenic non-methane volatile organic compounds (NMVOCs), ostensibly due to urbanization (De Smedt et al. 2010). Despite the overall positive trend in HCHO, some negative trends appear in Southern Africa during JJA and SON. Recent findings on emission decreases during Africa's peak fire season (Bauwens et al. 2016) may help explain these negative trends, including our result in Additional file 1: Figure S7. Considering that the largest CO decrease occurs in Southern Africa (Fig. 8), Southern Africa experiences a larger reduction of emissions from the biomass burning. This situation differs from the situation in South America, revealing a weaker CO decrease there while NO_2 and HCHO increase.

Conclusions

In this study, long-term satellite measurements of AOD, CO, NO_2, and HCHO in the Southern Hemisphere were used to investigate the spatiotemporal distribution of climatological mean and long-term trends. Additionally, the number of mid-latitudinal air masses that can be transported into the Antarctic region was determined using back trajectory simulations. AOD, CO, NO_2, and HCHO are typically high on the continents, and their extents vary among continents with the intensity and frequency of source events (e.g., biomass burning processes). However, even if the roles of these main sources are dominant, the spatial distributions of column magnitudes are not identical, due to compound-specific lifetime differences affecting the spatial ranges of diffusion and transport.

Combining these results with back trajectory calculations, we can evaluate the possibility that air pollutants from the mid-latitudes move into the Antarctic. The Jangbogo station does not seem to be influenced by pollutants from outside of Antarctica, due to a strong katabatic flow from the eastern Antarctic plateau. On the other hand, the intrusion of mid-latitudinal pollutants to the King Sejong station seems quite possible, and the Belgrano, Neumayer, and Syowa stations also show some moderate intrusions of mid-latitudinal air masses from South America. Meanwhile, the Davis station, located on the eastern Antarctic coast, is not strongly affected by meridional transport from South America. These findings indicate that meridional exchange between high latitudes and mid-latitudes differs among Antarctic regions. In order to better assess the contribution of mid-latitudinal air pollution to the polar atmospheric environment, further analyses are needed that can detect areas vulnerable to the intrusion of external air parcels.

Our analyses of long-term trends reveal that the magnitudes of the AOD, NO_2, and HCHO columns have been increasing in recent years, while the CO column has shown a decreasing pattern. The difference in trend

direction between AOD and CO suggests that the AOD increase is probably not mostly related to the biomass burning but rather to other factors. The NO_2 and HCHO increases strongly imply contributions of anthropogenic emissions, which probably will be more important in the future. Further detailed investigation of emission and chemical production processes in the Southern Hemisphere is needed in order to improve our understanding of the differences in trend direction between CO and the other compounds. The present study recommends the synthesis of observational reanalysis data with model simulations.

Additional files

Additional file 1: Figure S1. Seasonal mean pattern of 850-hPa wind field from NCEP-NCAR reanalysis data for (a) September-October-November (SON), (b) December-January-February (DJF), (c) March-April-May (MAM), and (d) June-July-August (JJA). **Figure S2.** The location of the King Sejong, Belgrano, Neumayer, Syowa, Davis, and Jangbogo stations around Antarctica. **Figure S3.** Monthly mean height variation of 10-day back trajectories arrived at 5 stations: For cases when back-trajectories come from the higher latitudes than the arrival site. Calculations for 2005-2016 were used. **Figure S4.** Same as Figure S3, but for cases when back-trajectories come from the lower latitudes than the arrival site. **Table S1.** Trends and their uncertainties of deseasonalized anomaly of AOD from 2005 to 2016. The regions having a significant trend are colored red (95% confidence level) or purple (90% confidence level). **Table S2.** As Table S1., but for CO. **Table S3.** As Table S1., but for NO2. **Table S4.** As Table S1., but for HCHO. **Figure S5.** Same as Fig. 6, but for the region (pixel) over 30-35°S in latitude and 22.5-67.5°W in longitude from 2005 to 2016. An example of time-series analysis at each pixel that we divided. **Figure S6.** Annual variation of seasonal mean wind speed for the region over 40-60°S in latitude and 22.5°W-22.5°E to explain the increasing trend of AOD in this region. **Figure S7.** Temporal variation of total fire counts (2005-2016) over South America (black), Africa (orange), and Australia (blue). (PDF 2090 kb)

Additional file 2: Data description used for auxiliary analysis. (PDF 148 kb)

Abbreviations

AMF: Air mass factor; AOD: Aerosol optical depth; BIRA-IASB: Belgian Institute for Space Aeronomy; DB: Deep blue; DOAS: Differential optical absorption spectroscopy; DT: Dark target; EOS: Earth Observing System; GDAS: Global Data Assimilation System; GOME: Global Ozone Monitoring Experiment; HYSPLIT: Hybrid Single-Particle Lagrangian Integrated Trajectory; LT: Local time; MODIS: Moderate Resolution Imaging Spectroradiometer; MOPITT: Measurements of Pollution in the Troposphere; NASA: National Aeronautics and Space Administration; NDVI: Normalized difference vegetation index; NIR: Near-infrared; NMVOC: Non-methane volatile organic compounds; OMI: Ozone Monitoring Instrument; PAN: Peroxyacetyl nitrates; SCD: Slant column density; TIR: Thermal-infrared; TOMS: Total Ozone Mapping Spectrometer; VCD: Vertical column density

Availability of data and materials

Not applicable

Authors' contributions

J-HK proposed the topic and designed the study. DHA and SSP carried out the experimental study. DHA, TC, S-JK, and J-HK performed the detailed analysis of results with the literature review. DHA, JK, and J-HK wrote the manuscript. All authors read and approved the final manuscript.

Competing interests

The authors declare that they have no competing interests.

Publisher's Note

Springer Nature remains neutral with regard to jurisdictional claims in published maps and institutional affiliations.

Author details

[1]Department of Atmospheric Sciences, Yonsei University, Seoul, Republic of Korea. [2]Korea Polar Research Institute, Incheon, Republic of Korea. [3]School of Earth and Environment Sciences, Seoul National University, Seoul, Republic of Korea. [4]Department of Atmospheric Sciences, Chungnam National University, Daejeon, Republic of Korea.

References

Bargagli R (2008) Environmental contamination in Antarctic ecosystems. Sci Total Environ 400(1–3):212–226 https://doi.org/10.1016/j.scitotenv.2008.06.062.

Bauwens M, Stavrakou T, De Smedt I, van Roozendael M, van der Werf GR, Wiedinmyer C, Kaiser JW, Sindelarova K, Guenther A (2016) Nine years of global hydrocarbon emissions based on source inversion of OMI formaldehyde observations. Atmos Chem Phys (ACP) 16(15) https://doi.org/10.5194/acp-16-10133-2016.

Beirle S, Platt U, Wenig M, Wanger T (2003) Weekly cycle of NO_2 by GOME measurements: a signature of anthropogenic sources. Atmos Chem Phys (ACP) 3:2225–2232 https://doi.org/10.5194/acp-3-2225-2003.

Bucsela EJ, Celarier EA, Wenig MO, Gleason JF, Veefkind JP, Boersma KF, Brinksma EJ (2006) Algorithm for NO_2 vertical column retrieval from the ozone monitoring instrument. IEEE Trans Geosci Remote Sens 44(5):1245–1258 https://doi.org/10.1109/TGRS.2005.863715.

Das S, Harshvardhan H, Bian H, Chin M, Curci G, Protonotariou AP, Mielonen T, Zhang K, Wang H, Liu X (2017) Biomass burning aerosol transport and vertical distribution over the south African-Atlantic region. J Geophys Res Atmos 122(12) https://doi.org/10.1002/2016JD026421.

De Meij A, Pozzer A, Lelieveld J (2012) Trend analysis in aerosol optical depths and pollutant emission estimates between 2000 and 2009. Atmos Environ 51:75–85 https://doi.org/10.1016/j.atmosenv.2012.01.059.

De Smedt I, Stavrakou T, Hendrick F, Danckaert T, Vlemmix T, Pinardi G, Theys N, Lerot C, Gielen C, Vigouroux C, Hermans C, Fayt C, Veefkind P, Müller JF, Van Roozendael M (2015) Diurnal, seasonal and long-term variations of global formaldehyde columns inferred from combined OMI and GOME-2 observations. Atmos Chem Phys (ACP) 15:12519–12545 https://doi.org/10.5194/acp-15-12519-2015.

De Smedt I, Stavrakou T, Muller JF, vad der ARJ, van Roozendael M (2010) Trend detection in satellite observations of formaldehyde tropospheric columns. Geophys Res Lett 37(18) https://doi.org/10.1029/2010GL044245.

De Smedt I, Van Roozendael M, Stavrakou T, Muller JF, Lerot C, Theys N, Valks P, Hao N, van der A R (2012) Improved retrieval of global tropospheric formaldehyde columns from GOWE-2/MetOp-A addressing noise reduction and instrumental degradation issues. Atmos Meas Tech (AMT) 5:2933–2949 https://doi.org/10.5194/amt-5-2933-2012.

Deeter MN, Edwards DP, Francis GL, Gille JC, Martinez-Alonso S, Worden HM, Sweeney C (2017) A climate-scale satellite record for carbon monoxide: the

MOPITT version 7 product. Atmos Meas Tech (AMT) 10(7):2533–2555 https://doi.org/10.5194/amt-10-2533-2017.

Deeter MN, Emmons LK, Francis GL, Edwards DP, Gille JC, Warner JX, Khattatov B, Ziskin D, Lamarque JF, Ho SP, Yudin V, Attie JL, Packman D, Chen J, Mao D, Drummond JR (2003) Operational carbon monoxide retrieval algorithm and selected results for the MOPITT instrument. J Geophys Res Atmos 108(D14): 4399–4409 https://doi.org/10.1029/2002JD003186.

Dufour G, Szopa S, Barkley MP, Boone CD, Perrin A, Palmer PI, Bernath PF (2009) Global upper-tropospheric formaldehyde: seasonal cycles observed by the ACE-FTS satellite instrument. Atmos Chem Phys (ACP) 9(12):3893–3910 https://doi.org/10.5194/acp-9-3893-2009.

Edwards DP, Emmons LK, Gille JC, Chu A, Attie JL, Giglio L, Wood SW, Haywood J, Deeter MN, Massie ST, Ziskin DC, Drummond JR (2006) Satellite-observed pollution from southern hemisphere biomass burning. J Geophys Res Atmos 111(D14) https://doi.org/10.1029/2005JD006655.

Fiebig M, Lunder CR, Stohl A (2009) Tracing biomass burning aerosol from South America to Troll Research Station, Antarctica. Geophys Res Lett 36(L14815) https://doi.org/10.1029/2009GL038531.

Gettelman A, Hoor P, Pan LL, Randel WJ, Hegglin MI, Birner T (2011) The extratropical upper troposphere and lower stratosphere. Rev Geophys 49(3) https://doi.org/10.1029/2011RG000355.

Gorodetskaya IV, Tsukernik M, Claes K, Ralph MF, Neff WD, Van Lipzig NPM (2014) The role of atmospheric rivers in anomalous snow accumulation in East Antarctica. Geophys Res Lett 41:6199–6206 https://doi.org/10.1002/2014GL060881.

Graf HF, Shirsat SV, Oppenheimer C, Jarvis MJ, Podzun R, Jacob D (2010) Continental scale Antarctic deposition of sulphur and black carbon from anthropogenic and volcanic sources. Atmos Chem Phys (ACP) https://doi.org/10.5194/acp-10-2457-2010.

Guenther A, Karl T, Harley P, Wiedinmyer C, Palmer PI, Geron C (2006) Estimates of global terrestrial isoprene emissions using MEGAN (model of emissions of gases and aerosols from nature). Atmos Chem Phys (ACP) 6:3181–3210 https://doi.org/10.5194/acp-6-3181-2006.

Hara K, Osada K, Yabuki M, Hashida G, Yamanouchi T, Hayashi M, Shiobara M, Nishita C, Wada M (2010) Haze episodes at Syowa Station, coastal Antarctica: where did they come from. J Geophys Res 115(D14205) https://doi.org/10.1029/2009JD012582.

Holloway T, Levy H II, Kasibhatla P (2000) Global distribution of carbon monoxide. J Geophys Res 105(D10):12123–12147 https://doi.org/10.1029/1999JD901173.

Hooghiemstra PB, Krol MC, van Leeuwen TT, van der Werf GR, Novelli PC, Deeter MN, Aben I, Röckmann T (2012) Interannual variability of carbon monoxide emission estimates over South America from 2006 to 2010. J Geophys Res 117(D15308) https://doi.org/10.1029/2012JD017758.

Hsu NC, Gautam R, Sayer AM, Bettenhausen C, Li C, Jeong MJ, Tsay SC, Holben BN (2012) Global and regional trends of aerosol optical depth over land and ocean using SeaWiFS measurements from 1997 to 2010. Atmos Chem Phys (ACP) 12(17):8037–8053 https://doi.org/10.5194/acp-12-8037-2012.

Huete A, Didan K, van Leeuwen W, Miura T, Glenn E (2010) MODIS vegetation indices. In: Ramachandran B, Justice C, Abrams M (eds) Land remote sensing and global environmental change. Remote sensing and digital image processing, vol 11. Springer, New York https://doi.org/10.1007/978-1-4419-6749-7_26.

Jones NB, Riedel K, Allan W, Wood S, Palmer PI, Chance K, Notholt J (2009) Long-term tropospheric formaldehyde concentrations deduced from ground-based fourier transform solar infrared measurements. Atmos Chem Phys (ACP) 9(18):7131–7142 https://doi.org/10.5194/acp-9-7131-2009.

Kishcha P, Starobinets B, Kalashnikova O, Long CN, Alpert P (2009) Variations of meridional aerosol distribution and solar dimming. J Geophys Res Atmos 114(D10) https://doi.org/10.1029/2008JD010975.

Kopacz M, Jacob DJ, Fisher JA, Logan JA, Zhang L, Megretskaia IA, Yantosca RM, Singh K, Henze DK, Burrows JP, Buchwitz M, Khlystova I, McMillan WW, Gille JC, Edwards DP, Eldering A, Thouret V, Nedelec P (2010) Global estimates of CO sources with high resolution by adjoint inversion of multiple satellite dataset (MOPITT, AIRS, SCIAMACHY, TES). Amos Chem Phys (ACP) 10:855–876 https://doi.org/10.5194/acp-10-855-2010.

Lamarque JF, Bond TC, Eyring V, Granier C, Heil A, Klimont Z, Lee D, Liousse C, Mieville A, Owen B, Schultz MG, Shindell D, Smith SJ, Stehfest E, Van Aardenne J, Cooper OR, Kainuma M, Mahowald N, McConnell JR, Naik V, Riahi K, van Vuuren DP (2010) Historical (1850–2000) gridded anthropogenic and biomass burning emissions of reactive gases and aerosols: methodology and application. Atmos Chem Phys (ACP) 10:7017–7039 https://doi.org/10.5194/acp-10-7017-2010.

Lamsal LN, Martin RV, Parrish DD, Krotkov NA (2013) Scaling relationship for NO2 pollution and urban population size: a satellite perspective. Environ Sci Technol 47(14):7855–7861 https://doi.org/10.1021/es400744g.

Leuchner M, Ghasemifard H, Lüpke M, Ries L, Schunk C, Menzel A (2016) Seasonal and diurnal variation of formaldehyde and its meteorological drivers at the GAW site Zugspitze. Aerosol Air Qual Res 16:801–815.

Levy RC, Mattoo S, Munchak LA, Remer LA, Sayer AM, Patadia F, Hsu NC (2013) The collection 6 MODIS aerosol products over land and ocean. Atmos Meas Tech (AMT) 6:2989–3034 https://doi.org/10.5194/amt-6-2989-2013.

Li C, Joiner J, Krotkov NA, Dunlap L (2015) A new method for global retrievals of HCHO total columns from the Suomi National Polar-orbiting Partnership Ozone Mapping and Profiler Suite. Geophys Res Lett 42:2515–2522 https://doi.org/10.1002/2015GL063204.

Li F, Ginoux P, Ramaswamy V (2008) Distribution, transport, and deposition of mineral dust in the Southern Ocean and Antarctica: contribution of major sources. J Geophys Res 113(D10207) https://doi.org/10.1029/2007JD009190.

Liu H, Jacob DJ, Bey I, Yantosca RM, Duncan BN, Sachse GW (2003) Transport pathways for Asian pollution outflow over the Pacific: interannual and seasonal variations. J Geophys Res 108(D20) https://doi.org/10.1029/2002JD003102.

Mao KB, Ma Y, Xia L, Chen WY, Shen XY, He TJ, Xu TR (2014) Global aerosol change in the last decade: an analysis based on MODIS data. Atmos Environ 94:680–686 https://doi.org/10.1016/j.atmosenv.2014.04.053.

McConnell JR, Maselli OJ, Sigl M, Vallelonga P, Neumann T, Anschutz H, Bales RC, Curran MAJ, Das SB, Edwards R, Kipfstuhl S, Layman L, Thomas ER (2014) Antarctic-wide array of high-resolution ice core records reveals pervasive lead pollution began in 1889 and persists today. Sci Rep 4(5848) https://doi.org/10.1038/srep05848.

McDonald BC, Dallmann TR, Martin EW, Harley RA (2012) Long-term trends in nitrogen dioxide emissions from motor vehicles at national, state, and air basin scales. J Geophys Res Atmos 117(D21) https://doi.org/10.1029/2012JD018304.

McKenzie RL, Seckmeyer G, Bais AF, Kerr JB, Madronich S (2001) J Geophys Res 106(D20):24051–24062 https://doi.org/10.1029/2001JD000545.

Mehta M, Singh R, Singh A, Singh N, Anshumali (2016) Recent global aerosol optical depth variations and trends—a comparative study using MODIS and MISR level 3 datasets. Remote Sens Environ 181:137–150. https://doi.org/10.1016/j.rse.2016.04.004.

Mok J, Park SS, Lim H, Kim J, Edward DP, Lee J, Yoon J, Lee YG, Koo JH (2017) Correlation analysis between regional carbon monoxide and black carbon from satellite measurements. Atmos Res 196(1):29–39 https://doi.org/10.1016/j.atmosres.2017.04.004.

Nazaryan H, McCormick MP, Menzel WP (2008) Global characterization of cirrus clouds using CALIPSO data. J Geophys Res Atmos 113(D16) https://doi.org/10.1029/2007JD009481.

Neff PD, Bertler NAN (2015) Trajectory modeling of modern dust transport to the Southern Ocean and Antarctica. J Geophys Res Atmos 120(18):9303–9322.

Ocko B, Ginoux PA (2017) Comparing multiple model-derived aerosol optical depth properties to spatially collocated ground-based and satellite measurements. Atmos Chem Phys (ACP) 17:4451–4475 https://doi.org/10.5194/acp-17-4451-2017.

Palmer PI, Abbot DS, Fu TM, Jacob DJ, Chance K, Kurosu TP, Guenther A, Wiedinmyer C, Stanton JC, Pilling MJ, Pressley SN, Lamb B, Sumner AL (2006) Quantifying the seasonal and interannual variability of North American isoprene emissions using satellite observations of the formaldehyde column. J Geophys Res 111(D12) https://doi.org/10.1029/2005JD006689.

Parish TR (1992) On the role of Antarctic katabatic winds in forcing large-scale tropospheric motions. J Atmos Sci 49(15):1374–1385.

Pereira K, Evanhelista H, Pereira E, Simões J, Johnson E, Melo L (2004) Transport of crustal microparticles from Chilean Patagonia to the Antarctic peninsula by SEM-EDS analysis. Tellus B 56(3):262–275 https://doi.org/10.1111/j.1600-0889.2004.00105.x.

Prospero JM, Ginoux P, Torres O, Nicholson SE, Gill TE (2002) Environmental characterization of global sources of atmospheric soil dust identified with the Nimbus 7 total ozone mapping spectrometer (TOMS) absorbing aerosol product. Rev Geophys 40(1) https://doi.org/10.1029/2000RG000095.

Sayer AM, Munchak LA, Hsu NC, Levy RC, Bettenhausen C, Jeong MJ (2014) MODIS collection 6 aerosol products: comparison between Aqua's e-deep blue, dark target, and "merged" data sets, and usage recommendations. J Geophys Res Atmos 119(24) https://doi.org/10.1002/2014JD022453.

Schneider P, Lahoz WA, Van der AR (2015) Recent satellite-based trends of tropospheric nitrogen dioxide over large urban agglomerations

worldwide. Atmos Chem Phys (ACP) 15:1205–1220 https://doi.org/10.5194/acp-15-1205-2015.

Shirsat SV, Graf HF (2009) An emission inventory of sulfur from anthropogenic sources in Antarctica. Atmos Chem Phys (ACP) 9(10):3397–3408.

Stavrakou T, Muller JF, De Smedt I, Van Roozendael M, van der Werf GR, Giglio L, Guenther A (2009) Global emissions of non-methane hydrocarbons deduced from SCIAMACHY formaldehyde columns through 2003-2006. Atmos Chem Phys 9:3663–3679 https://doi.org/10.5194/acp-9-3663-2009.

Stein AF, Draxler RR, Rolph GD, Stunder BJB, Cohen MD (2015) NOAA's HYSPLIT atmospheric transport and dispersion modeling system. Bull Am Meteorol Soc 96:2059–2077 https://doi.org/10.1175/bams-d-14-00110.1.

Stohl A, Sodemann H (2010) Characteristics of atmospheric transport into the Antarctic troposphere. J Geophys Res Atmos 115(D2) https://doi.org/10.1029/2009JD012536.

Streets DG, Shindell DT, Lu Z, Faluvegi G (2013) Radiative forcing due to major aerosol emitting sectors in China and India. Geophys Res Lett 40(16) https://doi.org/10.1002/grl.50805.

Té Y, Jeseck P, Franco B, Mahieu E, Jones N, Paton-Walsh C, Griffith DWT, Buchholz RR, Hadji-Lazaro J, Hurtmans D, Janssen C (2016) Seasonal variability of surface and column carbon monoxide over the megacity Paris, high-altitude Jungfraujoch and Southern Hemispheric Wollongong stations. Atmos Chem Phys (ACP) 16:10911–10925 https://doi.org/10.5194/acp-16-10911-2016.

Tomasi C, Kokhanovsky A, Lupi A, Ritter C, Smirnov A, O'Neill N (2015) Aerosol remote sensing in polar regions. Earth Sci Rev 140:108–157.

Torres O, Bhartia PK, Herman JR, Sinyuk A, Ginoux P, Holben B (2002) A long-term record of aerosol optical depth from TOMS observation and comparisons to AERONET measurements. J Atmos Sci 59:398–413.

Torres O, Chen Z, Jethva H, Ahn C, Freitas SR, Bhartia PK (2010) OMI and MODIS observations of the anomalous 2008-2009 southern hemisphere biomass burning seasons. Atmos Chem Phys 10(8):3505–3513 https://doi.org/10.5194/acp-10-3505-2010.

van der ARJ, Eskes HJ, Boersma KF, van Noije TPC, Van Roozendael M, De Smedt I, Peters DHMU, Meijer EW (2008) Trends, seasonal variability and dominant NO_x source derived from a ten year record of NO_2 measured from space. J Geophys Res 113(D04302) https://doi.org/10.1029/2007JD009021.

Wagner V, Glasow RV, Fischer H, Crutzen PJ (2002) Are CH2O measurements in the marine boundary layer suitable for testing the current understanding of CH_4 photooxidation?: A model study. J Geophys Res 107(D3) https://doi.org/10.1029/2001JD000722.

Wang T, Lam KS, Chan LY, Lee ASY, Carroll MA (1997) Trace gas measurements in coastal Hong Kong during the PEM-West B. J Geophys Res Atmos 102(D23) https://doi.org/10.1029/96JD03750.

Weatherhead EC, Reinsel GC, Tiao GC, Meng XL, Choi D, Cheang WK, Keller T, DeLuisi J, Wuebbles DJ, Kerr JB, Miller AJ, Oltmans SJ, Frederick JE (1998) Factors affecting the detection of trends: statistical considerations and applications to environmental data. J Geophys Res Atmos 103(D14):17149–17161 https://doi.org/10.1029/98JD00995.

Weller R, Minikin A, Petzold A, Wagenbach D, König-Langlo G (2013) Characterization of long-term and seasonal variations of black carbon (BC) concentrations at Neumayer, Antarctica. Atmos Chem Phys 13(3):1579–1590.

Weller R, Wagenbach D, Legrand M, Elsässer C, Tian-Kunze X, König-Langlo G (2011) Continuous 25-yr aerosol records at coastal Antarctica—I: inter-annual variability of ionic compounds and links to climate indices. Tellus B 63(5):901–919 https://doi.org/10.1111/j.1600-0889.2011.00542.x.

Wilson DI, Piketh SJ, Smirnov A, Holben BN, Kuyper B (2010) Aerosol optical properties over the South Atlantic and Southern Ocean during the 140th cruise of the M/V *S.A. Agulhas*. Atmos Res 98(2):285–296 https://doi.org/10.1016/j.atmosres.2010.07.007.

Worden HM, Deeter MN, Frankenberg C, George M, Nichitiu F, Worden J, Aben I, Bowman KW, Clerbaux C, Coheur PF, De Laat ATJ, Detweller R, Drummond JR, Edwards DP, Gille JC, Hurtmans D, Luo M, Martinez-Alonso S, Massie S, Pfister G, Warner JX (2013) Decadal record of satellite carbon monoxide observations. Atmos Chem Phys (ACP) 13(2):837–850 https://doi.org/10.5194/acp-13-837-2013.

Yurganov LN, Rakitin V, Dzhola A, August T, Fokeeva E, George M, Gorchakov G, Grechko E, Hannon S, Karpov A, Ott L, Semutnikova E, Shumsky R, Strow L (2011) Satellite- and ground-based CO total column observations over 2010 Russian fires: accuracy of top-down estimates based on thermal IR satellite data. Atmos Chem Phys (ACP) 11:7925–7942 https://doi.org/10.5194/acp-11-7925-2011.

Zeng G, Wood SW, Morgenstern O, Jones NB, Robinson J, Smale D (2012) Trends and variations in CO, C_2H_6, and HCN in the Southern Hemisphere point to the declining anthropogenic emissions of CO and C_2H_6. Atmos Chem Phys (ACP) 12:7543–7555 https://doi.org/10.5194/acp-12-7543-2012.

Zhang J, Reid JS, Holben BN (2005) An analysis of potential cloud artifacts in MODIS over ocean aerosol optical thickness products. Geophys Res Lett 32(15) https://doi.org/10.1029/2005GL023254.

Zhu L, Payne VH, Walker TW, Worden JR, Jiang Z, Kulawik SS, Fischer EV (2017) PAN in the eastern Pacific free troposphere: A satellite view of the sources, seasonality, interannual variability, and timeline for trend detection. J Geophys Res-Atmos 122:3614–3629 https://doi.org/10.1002/2016JD025868.